Hindawi
Complexity
Volume 2018, Article ID 2158391, 14 pages
https://doi.org/10.1155/2018/2158391

Research Article

Linear and Complex Measures of Heart Rate Variability during Exposure to Traffic Noise in Healthy Women

Myrela Alves,[1] David M. Garner,[2] Anne M. G. G. Fontes,[1] Luiz Vinicius de Alcantara Sousa,[3] and Vitor E. Valenti[1]

[1]*Centro de Estudos do Sistema Nervoso Autônomo, Departamento de Fonoaudiologia, Faculdade de Filosofia e Ciências, UNESP, Marília, SP, Brazil*
[2]*Cardiorespiratory Research Group, Department of Biological and Medical Sciences, Faculty of Health and Life Sciences, Oxford Brookes University, Headington, Oxford OX3 0BP, UK*
[3]*Laboratório de Epidemiologia e Análises de Dados, Faculdade de Medicina do ABC (FMABC), Santo Andre, SP, Brazil*

Correspondence should be addressed to Vitor E. Valenti; vitor.valenti@marilia.unesp.br

Received 1 October 2017; Revised 7 February 2018; Accepted 20 February 2018; Published 26 June 2018

Academic Editor: Gastón Schlotthauer

Previous studies have described significant impact of different types of noise on the linear behavior of heart rate variability (HRV). However, there are few studies regarding the complexity of HRV during exposure to traffic noise. In this study, we evaluated the complexity of HRV during traffic noise exposure. We analyzed 31 healthy female students aged between 18 and 30 years. Volunteers remained at rest seated under spontaneous breathing during 10 minutes with an earphone turned off, and then they were exposed to traffic noise through an earphone for a period of 10 minutes. The traffic noise was recorded from a very busy city street and the sound was comprised of car, bus, and trucks engines and horn (71–104 dB). We observed no significant changes in the linear analysis of HRV. CFP3 (Cohen's $d = 1.28$, large effect size) and CFP6 (Cohen's $d = 1.11$, large effect size) parameters of chaotic global analysis and Shannon (Cohen's $d = 1.13$, large effect size), Renyi (Cohen's $d = 1.06$, large effect size), and Tsallis (Cohen's $d = 1.14$, large effect size) entropies significantly *increased* ($p < 0.005$) during traffic noise exposure. In conclusion, traffic noise under laboratory conditions increased the complexity of HRV through chaotic global analysis and some measures of entropy in healthy females.

1. Introduction

Noise may be considered an unpleasant sound, which may have effects on physiological variables. It is often found in hazardous situations due to industrialization and urbanization [1]. In this way, the research literature has previously investigated the effects of different types of noise on autonomic nervous system by analyzing heart rate variability (HRV) [2]. Lee et al. [3] noted that white noise above 50 dB influences spectral analysis of HRV, indicating significant correlation between frequency domain analysis and sound pressure level. Umemura and Honda [4] restated that this type of noise also encourages deviations in HRV. Yet, until now the research literature has only focused on traditional linear indices of HRV analysis [2, 4, 5].

The linear analysis of HRV in the time and frequency domains is not entirely suitable to provide information about the complex dynamics of heartbeat origination. This is because the mechanisms involved in cardiovascular physiology interact with each other in a nonlinear way [6]. Furthermore, methods related to nonlinear behavior of HRV were reported to present clinical relevance and to offer improved interpretation about these pathological mechanisms [7, 8].

Most recently, the European Society of Cardiology together with the European Heart Rhythm Association and coendorsed by the Asia Pacific Heart Rhythm Society drew attention to nonlinear methods for assessing HRV [9]. In this review, the authors address entropy and regularity, long-range correlation and fractal analysis, short-term complexity, nonlinear dynamical systems, and chaotic behavior generally.

Nevertheless, there is little in the research literature comparing HRV analysis with chaotic global analysis and Shannon, Renyi, and Tsallis entropies (see later section on nonlinear analysis).

This information related to chaos theory, fractal mathematics, and the dynamic complexity of HRV has not yet been fully applied in medical practice clinically. Yet, it is a productive area for research and development of knowledge in both health and disease [10]. Besides, the complex measurement of the intervals between consecutive heart beats (RR intervals) analysis during exposure to traffic noise has not been studied. Studies analyzing HRV and traffic noise exposed subjects to real traffic, which exposed subjects to multiple stimuli (visual, conversation, temperature, and humidity) that have a significant impact on the autonomic nervous system. Sensitive techniques to identify autonomic changes are necessary to avert possible physiological injury in the organism. Consequently, we aimed to evaluate the acute effects of traffic noise on the complexity of HRV under *laboratory* conditions alone.

2. Method

2.1. Study Population. We examined 31 apparently healthy female students aged between 18 and 30 years. All volunteers were informed about the procedures and objectives of the study and, after agreeing, signed a confidential consent form. All study procedures were approved by the Research Ethics Committee (REC) of the institution (case number 2011/382) and followed the Resolution 196/96 of the National Health Council. We excluded women under the following conditions: body mass index (BMI) > 30 kg/m^2, systolic blood pressure (SBP) > 140 mmHg or diastolic blood pressure (DBP) > 90 mmHg (at rest), and endocrine, cardiovascular, respiratory, and neurological related disorders or any condition that prevented the subject from performing the study. In order to avoid effects related to sexual hormones, we did not include women on the 11th to 15th and 21st to 25th days after the first day of the menstrual cycle [11].

2.2. Initial Assessment. The subjects were identified by collecting the following information: age, mass, height, and body mass index (BMI). Mass was measured using a digital scale (W200/5, Welmy, Brazil) with a precision of 0.1 kg. Height was determined using a stadiometer (ES2020, Sanny, Brazil) with a precision of 0.1 cm and being 220 cm long. The body mass index (BMI) was calculated by the subsequent formula: mass (kg)/height (m^2). We measured heart rate and blood pressure. Heart rate was measured with the Polar RS800CX heart rate monitor (Polar Electro, Finland). Blood pressure was indirectly measured by auscultation through calibrated aneroid sphygmomanometer (Welch Allyn, New York, USA) and stethoscope (Littmann, St. Paul, USA) with all subjects seated.

2.3. Measurement of Auditory Stimulation. The measurements of equivalent sound levels were performed in a soundproofed room, using an audio dosimeter SV 102 (Svantek, Finland). It was programmed in measuring circuit 7 in "A" weighting, slow response [12].

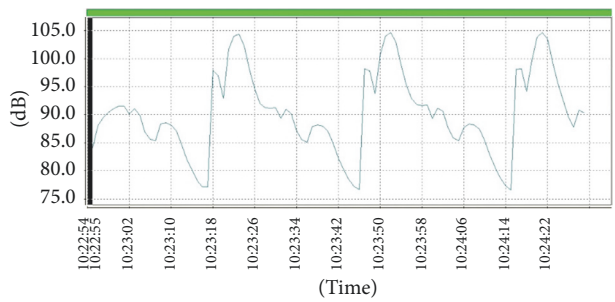

Figure 1: Equivalent sound level.

We used the MIRE earphone, which was placed inside the auditory canal of the subject and linked to a personal stereo. Prior to each measurement, the earphones were calibrated with the acoustic calibrator CR: Model 514 (Cirrus Research plc).

This tool was used to analyze the Leq (A), which is defined as the equivalent sound pressure level, and the sound level corresponds to the same constant time interval. It contained the same total sound energy, which also analyzed the spectrum of sound stimulation (eighth track) frequency [13] of traffic noise (71–104 dB) (Figure 1).

2.4. Experimental Protocol. Data collection was commenced at room temperature between 21°C and 25°C and with humidity between 50% and 60%. The subjects were instructed not to ingest alcohol or caffeine for 24 hours prior to evaluation. The data collection was achieved individually between 18:00 and 21:00 to avoid circadian influences. The volunteers were instructed to remain at rest and avoid conversation during the experiment.

After the initial evaluation, the heart monitor belt was placed over the thorax, aligned with the distal third of the sternum and the Polar RS800CX heart rate receiver (Polar Electro, Finland) was placed on the wrist. Subsequently, the volunteers remained at rest seated for 10 minutes with the headset off.

Next, the volunteers were exposed to traffic noise through an earphone for a period of 10 minutes. The traffic noise was recorded from a very busy street in Marília city, SP, Brazil. The sounds were produced by cars, buses, trucks engineers, and horns.

2.5. Analysis of HRV. The RR intervals were recorded by the Polar RS800CX heart rate monitor with a sampling rate of 1000 Hz. They were then transferred to the Polar Precision Performance software (v. 3.0, Polar Electro, Finland). This software allowed the visualization of the HR and the extraction of a file relating to a cardiac period (RR-interval) in a "txt" file. After digital filtering supplemented with manual filtering to eliminate artefacts and premature ectopic beats, 500 RR intervals were applied for data analysis. Only series with more than 95% of sinus beats were included in the study. HRV was analyzed before and during traffic noise.

2.6. Linear Analysis of HRV. The time domain analysis was accomplished in terms of SDNN (standard deviation of normal-to-normal RR intervals), pNN50 (percentage of adjacent RR intervals with a difference of duration greater than 50 milliseconds), and RMSSD (root-mean square of differences between adjacent normal RR intervals in a time interval) [14].

To obtain the spectral indexes for HRV analysis in the frequency domain, the frequency recordings underwent mathematical processing, thus generating a tachogram that expressed the variation of RR intervals as a function of time. The tachogram contained a signal that varied with time and was processed by the mathematical Fast Fourier Transform (FFT) algorithm. Welch's periodogram method based on FFT using a window width of 256 seconds and an overlap of 50% was applied.

Low frequency (LF, ranging between 0.04 and 0.15 Hz) and high frequency (HF, ranging from 0.15 to 0.4 Hz) spectral components were selected in normalized units (nu). The ratio between these components in absolute values (LF/HF) represents the relative value of each spectral component in relation to the total potential minus the very low frequency (VLF) components. It is important to mention that the LF/HF index may provide significant information on autonomic regulation of sinus node under controlled conditions and short-term recordings [14].

For computation of the linear indices, we applied the HRV analysis software (Kubios HRV v.1.1 for Windows, Biomedical Signal Analysis Group, Department of Applied Physics, University of Kuopio, Finland).

2.7. Statistical Analysis of Linear Indices. Statistical methods of the linear indices were approved for the computation of means and standard deviations. Normal Gaussian distribution of the data was verified by the Shapiro-Wilk goodness-of-fit test (z value > 1.0).

To enable a comparison of the variables between control and traffic noise exposure, we applied the unpaired Student t-test for parametric distribution and the Mann–Whitney test for nonparametric distributions. Level of significance was set at $p < 0.005$, 0.5%.

2.8. Nonlinear Analysis

2.8.1. Detrended Fluctuation Analysis (DFA). Detrended fluctuation analysis (DFA) [15] may be applied to datasets where parameters such as mean, variance, and autocorrelation vary with time. DFA computes the correlation *within* the signal. It quantifies how the fluctuations of a signal scale with the number of samples of that signal. According to Donaldson et al. [16], the time series of length k was manipulated as shown:

$$y(k) = \sum_{i=1}^{k} (\mathrm{RR}(i) - \mathrm{mean}(\mathrm{RR})). \quad (1)$$

The integrated time series was then divided into equally sized and nonoverlapping windows of length w. A linear regression line was fitted through the data in each window and the time series manipulated by subtracting the regression line from the data.

The root-mean square fluctuation $F(w)$ of the integrated and detrended time series was calculated for different values of w, as follows:

$$F(w) = \left[\frac{1}{N} \sum_{k=1}^{N} \left[y(k) - y_w(k) \right]^2 \right]^{1/2}. \quad (2)$$

The scaling exponent (α) was obtained as the slope of a straight line fit to $F(w)$ against w on a log-log plot:

$$F(w) \propto w^{\alpha}. \quad (3)$$

DFA is a technique extensively imposed in variability analysis. It has been applied to the evaluation of posture [17], exercise [18] and sleep stage classification [19], and classification of asthma [20] and COPD [16, 21, 22].

2.8.2. Chaotic Global Analysis. Multitaper Method (MTM) [23] is useful for spectral estimation and signal reconstruction, of a time series of a spectrum that may contain broadband and line components. MTM lessens the variances of spectral estimates by using a small set of tapers (windows). Data is premultiplied by orthogonal tapers created to minimize the spectral leakage owing to the finite length of the time series. A set of approximations of the power spectrum are calculated. These functions identified as Discrete Prolate Spheroidal Sequences (DPSS) sometimes called Slepian Sequences [24] are a set of functions which optimize these tapers. They are defined as eigenvectors of a Rayleigh-Ritz minimization problem [25].

2.8.3. High Spectral Entropy. High spectral entropy (*hs*Entropy) [26] is a function of the irregularity of amplitude and frequency of the power spectra peaks. It is derived by applying Shannon entropy to the MTM power spectrum (see Figure 2). Then, we calculate an intermediate parameter which is the median Shannon entropy of the value obtained from three different power spectra using the MTM power spectra under three test conditions: (a) a perfect sine wave, (b) uniformly distributed random variables, and finally (c) the experimental oscillating signal. These values are normalized mathematically so that the sine wave gives a value of zero, uniformly random variables give unity, and the experimental signal gives values between zero and unity. It is the final value that corresponds to *hs*Entropy.

2.8.4. High Spectral DFA. As stated before, the DFA [26] algorithm can be applied to datasets where statistics such as mean, variance, and autocorrelation vary with time. The *high spectral* detrended fluctuation analysis (*hs*DFA) algorithm is where the DFA is applied to the frequency rather than time on the horizontal axis (Figure 2). So, the x-axis is frequency and the y-axis is amplitude. To obtain *hs*DFA, we calculate the spectral adaptation in exactly the same manner as for *hs*Entropy applying a MTM power spectrum with the same settings, but DFA rather than Shannon entropy is the algorithm enforced.

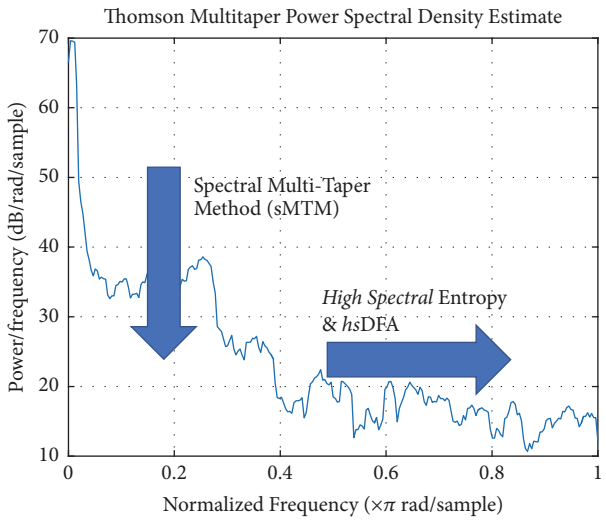

Figure 2: A MTM power spectrum of a time series of 500 RR intervals in a traffic noise exposure subject. sMTM is the area beneath the spectrum, yet above the baseline created by broadband noise as the signal becomes chaotic. *High spectral* entropy and *high spectral* DFA are derived by applying the Shannon entropy and detrended fluctuation analysis (DFA) functions to the MTM power spectrum. Parameters for the MTM power spectra as set at (i) sampling frequency of 1 Hz, (ii) time bandwidth for the DPSS at 3, (iii) FFT length of 256, and (iv) Thomson's *"adaptive"* nonlinear combination method to combine individual spectral estimates.

2.8.5. Spectral Multitaper Method. Spectral Multitaper Method (sMTM) [27] is founded on the increased intensity of broadband noise in power spectra generated by irregular and chaotic signals. sMTM is the area between the MTM power spectrum and the baseline (see Figure 2).

2.8.6. Chaotic Forward Parameters (CFP 1 to CFP7). The parameters (CFP 1–7) are referred to as chaotic forward parameters (CFP) for the functions CFP1 to CFP7 below where they are applied to normal and traffic noise exposure subjects' RR-interval time series. Since *hs*DFA responds to chaos inversely to the others, we subtract its value from unity. In this study, all three chaotic global values have weightings of unity.

$$\begin{aligned}
\text{CFP1} &= \left[\left(\left[\frac{hs\text{Entropy}}{\max(hs\text{Entropy})}\right]\right)^2 + \left(\left[\frac{\text{sMTM}}{\max(\text{sMTM})}\right]\right)^2 + \left(1 - \left[\frac{hs\text{DFA}}{\max(hs\text{DFA})}\right]\right)^2\right]^{1/2} \\
\text{CFP2} &= \left[\left(\left[\frac{hs\text{Entropy}}{\max(hs\text{Entropy})}\right]\right)^2 + \left(1 - \left[\frac{hs\text{DFA}}{\max(hs\text{DFA})}\right]\right)^2\right]^{1/2} \\
\text{CFP3} &= \left[\left(\left[\frac{hs\text{Entropy}}{\max(hs\text{Entropy})}\right]\right)^2 + \left(\left[\frac{\text{sMTM}}{\max(\text{sMTM})}\right]\right)^2\right]^{1/2} \\
\text{CFP4} &= \left[\left(\left[\frac{\text{sMTM}}{\max(\text{sMTM})}\right]\right)^2 + \left(1 - \left[\frac{hs\text{DFA}}{\max(hs\text{DFA})}\right]\right)^2\right]^{1/2} \\
\text{CFP5} &= \left|\left(1 - \left[\frac{hs\text{DFA}}{\max(hs\text{DFA})}\right]\right)\right| \\
\text{CFP6} &= \left|\left(\left[\frac{\text{sMTM}}{\max(\text{sMTM})}\right]\right)\right| \\
\text{CFP7} &= \left|\left(\left[\frac{hs\text{Entropy}}{\max(hs\text{Entropy})}\right]\right)\right|.
\end{aligned} \tag{4}$$

2.8.7. Shannon Entropy. Shannon entropy [28] is represented by the degree of ambiguity associated with the occurrence of the result. A higher value of entropy gives a more uncertain outcome and is more difficult to predict.

Shannon entropy may be used globally, applying to the time series wholly or nearby around specific points. This measure can provide extra evidence about specific events such as outliers or intermittent events. In contrast to Tsallis [29] and Renyi [30] entropies, Shannon entropy is additive. Hence, if the probabilities can be factorised into independent factors, the entropy of the joint process is the sum of the entropies of the distinct processes.

2.8.8. Renyi Entropy. Renyi entropy is a general statement of Shannon entropy that is dependent on a specified parameter. Renyi entropy depends on the entropic order α (which we set to 0.25). Renyi entropy approaches Shannon entropy as $\alpha \to 1$ which can be derived by l'Hôpital's rule [31, 32]. As entropic order increases, the procedures become more sensitive to the values occurring at higher probabilities and less sensitive to those of lower probabilities. Renyi entropy is described fully in studies by Zyczkowski [33] and Lenzi et al. [30].

2.8.9. Tsallis Entropy. Tsallis entropy is a general statement of the standard Shannon-Boltzmann-Gibbs entropy. It was introduced in the application of statistical mechanics and is used in computer sciences for pattern recognition. Tsallis entropy is dependent on the specified parameter termed entropic index q (which we set to 0.25); Tsallis entropy becomes the Shannon-Boltzmann-Gibbs entropy, as the entropic index $q \to 1$. Tsallis entropy is discussed further in the publications by dos Santos [29], A. R. Plastino and A. Plastino [34], and Mariz [35].

2.8.10. Approximate Entropy. Approximate Entropy (ApEn) was discussed by Pincus [36]. It is a procedure required

to evaluate the level of uniformity and the unpredictability of changes over time series. ApEn is the logarithmic ratio of component-wise matching sequences from the signal length, N. Other parameters include r, tolerance, and m, the embedding dimension. Here we set the parameters of m to 2 and r to 20% of the standard deviation of the data. The disadvantages of ApEn are that it is very dependent on the length of the time series and is often lower than expected on shorter time series. Finally, it is disadvantageous because it lacks "relative consistency" [37].

A minimum value of zero for ApEn would indicate a totally predictable time series, while a maximum value of one would specify an entirely unpredictable time series. Most of the time, the values are between these two values.

ApEn is mathematically described as in the Kubios HRV Analysis Manual [38].

First a set of length m vectors u_j is formed; note the embedding dimension, m, and N, the number of RR intervals.

$$u_j = \left(\mathrm{RR}_j, \mathrm{RR}_{j+1}, \ldots, \mathrm{RR}_{j+m-1}\right), \quad j = 1, 2, \ldots, N - m + 1. \tag{5}$$

The distance between these vectors is the maximum absolute difference between the corresponding elements; hence,

$$d\left(u_j, u_k\right) = \max\left\{\left|\mathrm{RR}_{j+n} - \mathrm{RR}_{k+n}\right| \mid n = 0, \ldots, m-1\right\}. \tag{6}$$

Next for each u_j the relative number of vectors u_k for which $d(u_j, u_k) \leqslant r$ is calculated. This index is denoted with $C_j^m(r)$ and can be written in the form

$$C_j^m(r) = \frac{\text{number of}\left\{u_k \mid d\left(u_j, u_k\right) \leqslant r\right\}}{N - m + 1} \quad \forall k. \tag{7}$$

Due to the normalization, the value of $C_j^m(r)$ is always smaller than or equal to 1. Note that the value is, however, at least $1/(N - m + 1)$ since u_j is also included in the count. Then, take the natural logarithm of each $C_j^m(r)$ and average over j to yield

$$\Phi^m(r) = \frac{1}{N - m + 1} \sum_{j=1}^{N-m+1} \ln C_j^m(r). \tag{8}$$

Finally, the ApEn is obtained as $\mathrm{ApEn}(m, r, N) = \Phi^m(r) - \Phi^{m+1}(r)$.

2.8.11. Sample Entropy. Sample entropy (SampEn) [37–39] is analogous to ApEn but there are two significant modifications in its computation. For ApEn, in the computation of the number of vectors u_k for which $d(u_j, u_k) \leqslant r$, also the vector u_j itself is contained within. This ensures that $C_j^m(r)$ is always greater than zero and the logarithm can be calculated. Regrettably, it makes ApEn biased. SampEn was formulated to lessen this bias. Yet again, the embedding dimension is m and the tolerance parameter r. We set m to 2 and r to 20% of the standard deviation of the time series. Equally, ApEn and SampEn are estimations for the negative natural logarithm of the conditional probability that data of length N, having repeated itself within a tolerance r for m points, will also repeat itself for $m + 1$ points.

SampEn is also described as in the Kubios HRV Analysis Manual [38].

In SampEn, the self-comparison of u_j is eliminated by calculating $C_j^m(r)$ as

$$C_j^m(r) = \frac{\text{number of}\left\{u_k \mid d\left(u_j, u_k\right) \leqslant r\right\}}{N - m} \quad \forall k \neq j. \tag{9}$$

Now the value of $C_j^m(r)$ will be between 0 and 1. Then, the values of $C_j^m(r)$ are averaged to yield

$$C^m(r) = \frac{1}{N - m + 1} \sum_{j=1}^{N-m+1} C_j^m(r). \tag{10}$$

SampEn is described mathematically as $\mathrm{SampEn}(m, r, N) = \ln(C^m(r)/C^{m+1}(r))$.

2.8.12. Higuchi Fractal Dimension (HFD). Fractal systems exhibit a characteristic termed self-similarity. A self-similar object upon close examination is comprised of smaller versions of itself. There are several algorithms which can be applied to measure fractal dimension. There are those by Higuchi [40], Katz [41], and Castiglioni [42]. Here, we apply the technique formulated by Higuchi viewed frequently as the most robust technique.

Higuchi derived this new algorithm to measure the fractal dimension of discrete time sequences. It is a technique that is enforced directly to the RR intervals. There is no power spectrum step involved. As the reconstruction of the attractor phase space is unnecessary, the algorithm is simpler and faster than the Correlation Dimension [43, 44]. Khoa et al. [45] describe the algorithm mathematically, adapted below.

It is based on a measure of length, $L(k)$, of the curve that represents the considered time series while using a segment of k samples as a unit, if $L(k)$ scales like

$$L(k) \sim k^{-D_f}. \tag{11}$$

The curve is said to show fractal dimension D_f because a simple curve has dimension equal to 1 and a plane has dimension equal to 2; value of D_f is always between 1 (simple curve) and 2 (curve which almost fills out the whole plane). D_f measures complexity of the curve and so of the time series this curve represents on a graph.

From a given time series, $\mathrm{RR}(1), \mathrm{RR}(2), \ldots, \mathrm{RR}(N)$, the algorithm constructs k new time series:

$$\mathrm{RR}_{km} = \left\{\mathrm{RR}(m), \mathrm{RR}(m+k), \mathrm{RR}(m+2k), \ldots, \mathrm{RR}\left(m + \mathrm{int}\left(\frac{(N-m)}{k}\right) \cdot k\right)\right\} \quad \text{for } m = 1, 2, \ldots, k, \tag{12}$$

Table 1: Body mass index (BMI), age, height, and mass of the volunteers. m: meters; kg: kilograms; bpm: beats per minute; ms: milliseconds; mmHg: millimeters of mercury.

Variable	Value
Age (years)	20.5 ± 1.4
Height (m)	1.62 ± 0.5
Mass (kg)	59.9 ± 12.1
BMI (kg/m^2)	22.7 ± 4.5

where m is initial time value, k indicates the discrete time interval between points (hence the delay, $k_{\max}$, is the maximum interval time), and int(a) is integer part of a real number a.

For each of the time series RR_{km} constructed, the average length $L_m(k)$ is then computed as

$$L_m(k) = \frac{1}{k}\left[\left(\sum_{i=1}^{\mathrm{int}((N-m)/k)} |\mathrm{RR}(m+i\cdot k) - \mathrm{RR}(m+(i-1)\cdot k)|\right)\right] \times \frac{N-1}{\mathrm{int}((N-m)/k)\cdot k}, \quad (13)$$

where N is total number of RR intervals. Afterwards, the length of the curve for time interval k is expressed as the sum value over k sets of $L_m(k)$ as illustrated by the following equation:

$$L(k) = \frac{1}{k}\sum_{m=1}^{k} L_m(k). \quad (14)$$

Finally, the slope of the curve $\ln(L(k))/\ln(1/k)$ is estimated using least squares linear best fit and the resulting slope is the HFD. To select a suitable value for $k_{\max}$, HFD values are plotted against a range of $k_{\max}$. The point at which the fractal dimension plateaus is considered a saturation point. That $k_{\max}$ value should be selected. No saturation point is achieved with the data we measured here.

2.8.13. Effect Size. To quantify the magnitude of difference between protocols for significant differences, the effect size was calculated using Cohen's d for significant differences ($p < 0.005$). Effect size was considered large for values ≥ 0.9, medium for values between 0.9 and 0.5, and small for values between 0.5 and 0.25 [46].

3. Results

Table 1 illustrates the values for mass, height, and BMI of the volunteers; all values were within normal physiological standards.

According to Figures 3 and 4, we illustrate that traffic noise did not induce significant changes in linear indices of HRV analysis. There was no significant change in the time (heart rate, SDNN, Mean RR, pNN50, and RMSSD) and frequency domain (LF and HF in absolute and normalized units and LF/HF ratio) indices of HRV.

3.1. Chaotic Global Analysis. In Table 2 and Figure 5, we display mean values and standard deviation for the chaotic forward parameters (CFP1 to CFP7) for the normal and traffic noise exposure subjects. There are 500 RR intervals throughout and both the parametric one-way analysis of variance (ANOVA1) and the nonparametric Kruskal-Wallis tests of significance are applied. The following are the inconclusive tests of normality (see below).

There are seven permutations of the three chaotic global parameters. All chaotic global values have equal weighting. The chaotic forward parameter (CFP) enables different combinations of chaotic globals to be applied to ensure that we have the best combination to be verified later by a multivariate analysis. It is anticipated that the CFP which applies all three should be the most robust. This is because it takes the information and processes it in three different ways. The summation of the three would be expected to deviate greater than single or double permutations. The potential analytical hazard here is that since we are only calculating spectral components, the phase information is lost.

When implementing parametric statistics, normal distribution of data is assumed. To test this assumption, we apply the Anderson-Darling and Lilliefors tests. In the case of the Anderson-Darling test, an empirical cumulative distribution function is applied, while the Lilliefors test is beneficial when the number of subjects is low. The results from both tests reveal similar numbers of nonnormal and normal distributions, so we apply both the Kruskal-Wallis and ANOVA1 tests of significance.

3.2. Principal Component Analysis. Principal Component Analysis (PCA) is a multivariate technique for analyzing the complexity of high-dimensional datasets. PCA is useful when (1) sources of variability in the data need to be explained and (2) reducing the complexity of the data and through this assessing the data with less dimensions. The primary goal of PCA is to rationalize the sources of variability in the data and to represent the data with fewer variables while sustaining the majority of the total variance (Figure 6).

CFP1t has the First Principal Component (PC1) of 0.358 and the Second Principal Component (PC2) of −0.406. However, CFP3t has PC1 of 0.191 and PC2 of −0.540. Only the first two components need be considered due to the steep scree plot. The cumulative influence as a percentage is 58.1 percent for the PC1 and 99.5 percent for the cumulative total of the PC1 and PC2. PC2 has an influence of 41.3 percent. So, CFP1 which applies all three chaotic global techniques is the optimal and most robust overall combination regarding influencing the correct outcome (Figure 6).

Table 3 illustrates the relevant Principal Component Analysis for CFPt for 7 groups of 31 traffic noise exposure subjects. The CFP values are deduced from RR-interval time series and with the chaotic global algorithms enforced.

3.3. Higuchi Fractal Dimension (HFD). The descriptive statistics of the Higuchi fractal dimension from the control subjects ($N = 31$) for 500 RR intervals are presented in Table 4. The parameter was calculated repeatedly for values of $K_{\max}$ between 10 and 150 at intervals of 10.

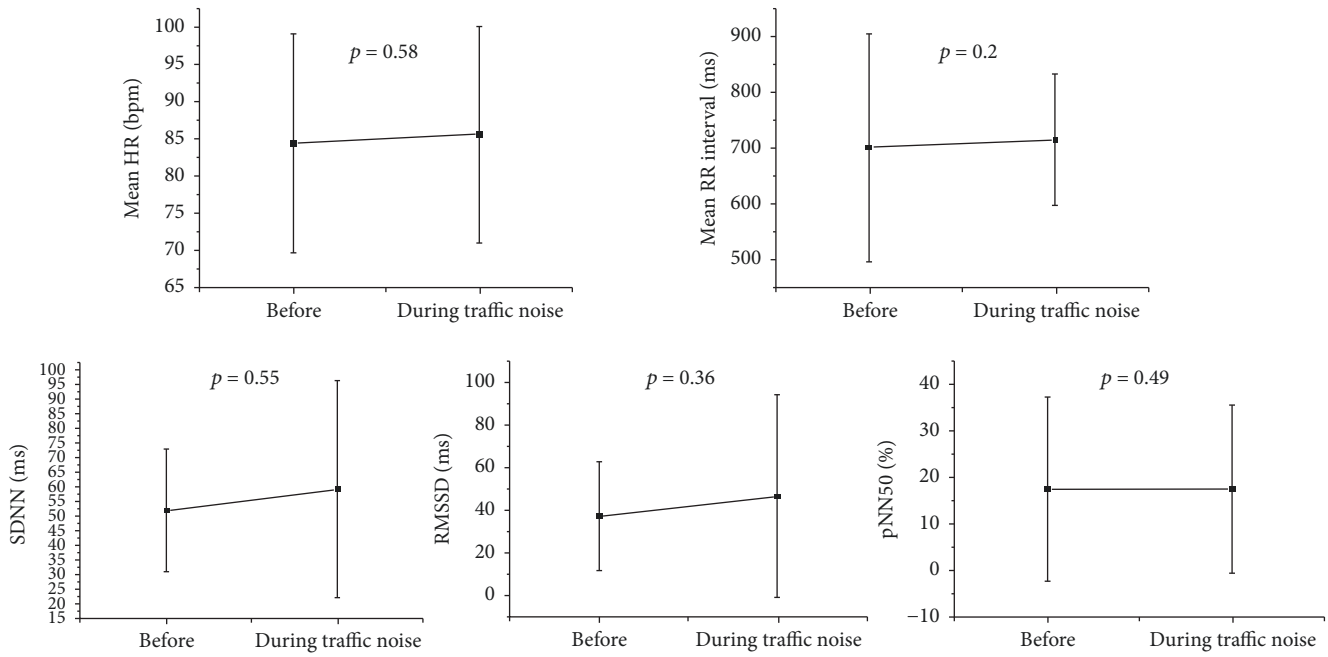

Figure 3: Mean heart rate and HRV analysis before (control) and during traffic noise exposure. pNN50: the percentage of adjacent RR intervals with a difference of duration greater than 50 ms; RMSSD: root-mean square of differences between adjacent normal RR intervals in a time interval; SDNN: standard deviation of normal-to-normal RR intervals; HR: heart rate; p: level of significance.

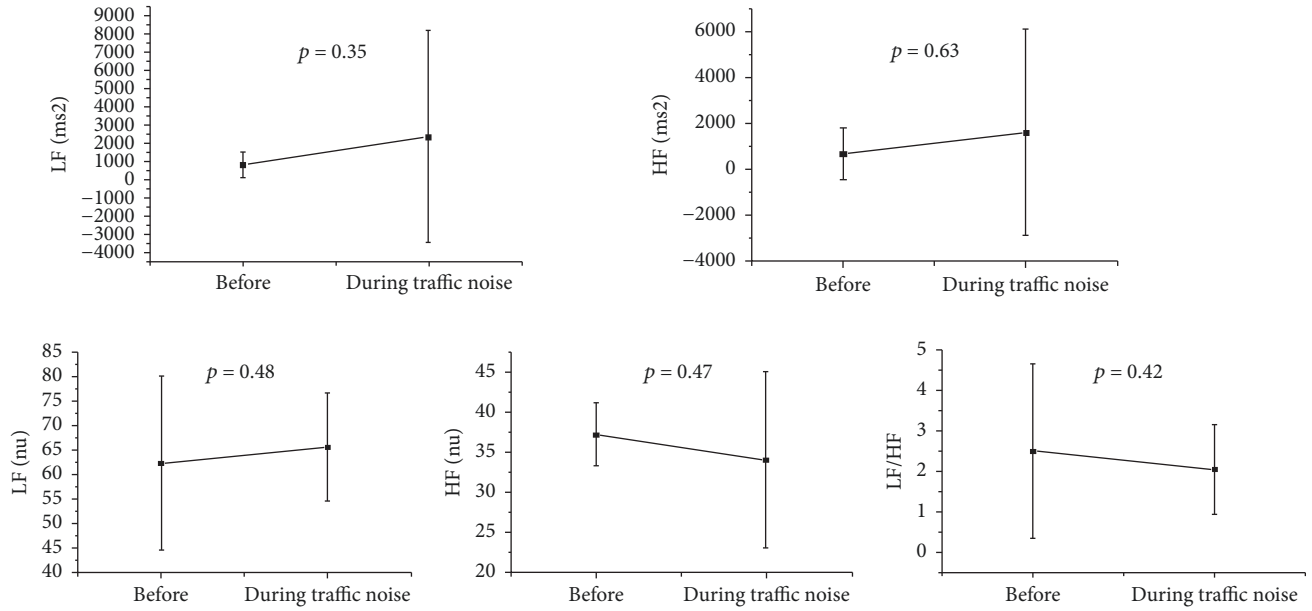

Figure 4: HRV analysis before (control) and during traffic noise exposure. LF: low frequency; HF: high frequency; LF/HF: low frequency/high frequency ratio; n.u.: normalized units; ms: milliseconds; HR: heart rate; p: level of significance.

The descriptive statistics of the Higuchi fractal dimension from the traffic noise exposure subjects ($N = 31$) for 500 RR intervals are presented in Table 5. The parameter was calculated repeatedly for values of $K_{\max}$ between 10 and 150 at intervals of 10.

Figure 7 illustrates the box-and-whiskers plot for Higuchi fractal dimension of RR intervals of the control subjects (a) and the traffic noise exposure subjects (b), calculated multiple times from 10 to 150 in equidistant units for different levels of $K_{\max}$. The point closest to the zero is the minimum and the point farthest away is the maximum. The boundary of the box closest to zero indicates the 25th percentile, a line within the box marks the median (not the mean), and the boundary of the box farthest from zero indicates the 75th percentile.

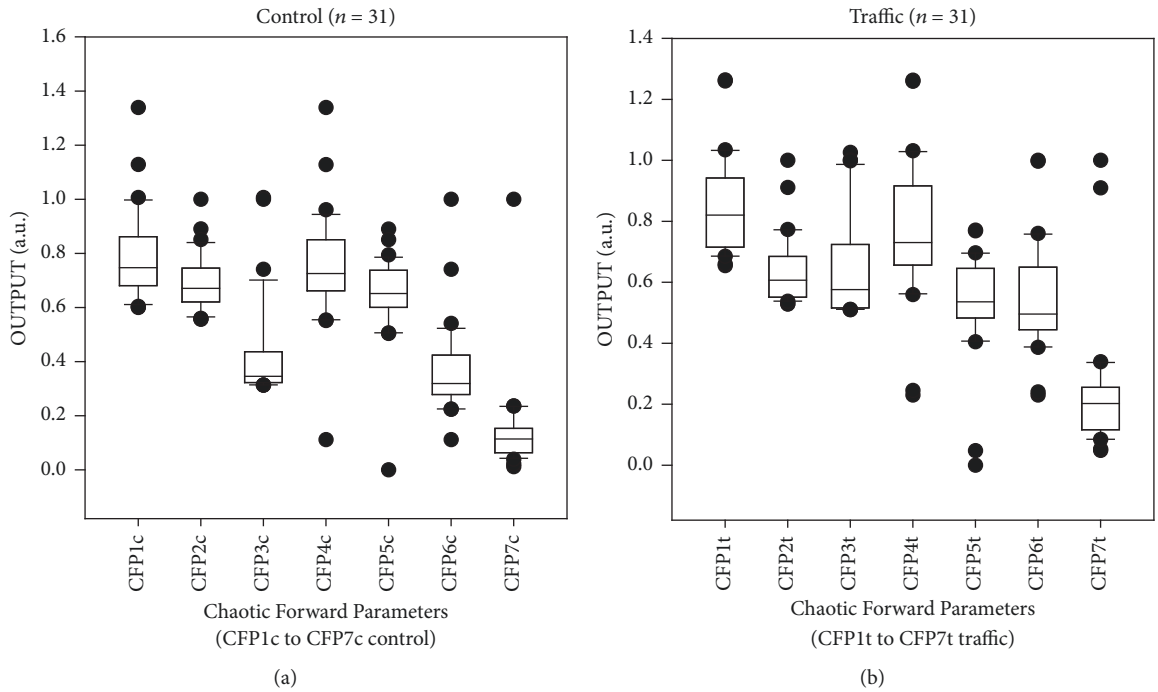

Figure 5: The boxplots illustrate the values of chaotic forward parameters one to seven (CFP1 to CFP7) for control (a) and traffic noise exposure (b) subjects with 500 RR intervals throughout. The point closest to the zero is the minimum and the point farthest away is the maximum. The boundary of the box closest to zero indicates the 25th percentile, a line within the box marks the median (not the mean), and the boundary of the box farthest from zero indicates the 75th percentile. The difference between these points is the interquartile range (IQR). Whiskers (or error bars) above and below the box indicate the 90th and 10th percentiles, respectively.

Table 2: Mean values and standard deviation for the chaotic forward parameters (CFP) for the normal and traffic noise exposure subjects.

Chaotic global	Mean ± SD Normal (n = 31)	Mean ± SD Traffic (n = 31)	ANOVA1 (p value)	Kruskal-Wallis (p value)	Effect size
CFP1	0.7853 ± 0.1602	0.8491 ± 0.1620	0.1243	0.0704	-
CFP2	0.6889 ± 0.1003	0.6325 ± 0.1105	0.0395	0.0043	0.53 (medium)
CFP3	0.4182 ± 0.1790	0.6368 ± 0.1598	<0.0001	<0.0001	1.28 (large)
CFP4	0.7439 ± 0.2022	0.7749 ± 0.2281	0.5739	0.4182	-
CFP5	0.6428 ± 0.1524	0.5376 ± 0.1676	0.0121	0.0011	0.65 (medium)
CFP6	0.3620 ± 0.1646	0.5517 ± 0.1764	<0.0001	<0.0001	1.11 (large)
CFP7	0.1440 ± 0.1698	0.2316 ± 0.2084	0.0748	0.0016	0.46 (small)

Table 3: Principal Component Analysis for CFPt for 7 groups of 31 traffic noise exposure subjects.

Chaotic global	PC1	PC2
CFP1t	0.358	−0.406
CFP2t	0.066	−0.577
CFP3t	0.191	−0.540
CFP4t	0.490	0.086
CFP5t	0.446	0.253
CFP6t	0.494	−0.023
CFP7t	−0.384	−0.371

Table 4: Higuchi fractal dimension statistics through K_{max} between 10 and 150 at intervals of 10 in the control protocol.

Property	Higuchi fractal dimension Statistics (control)							
K_{max}	Mean	SE mean	StDev	Minimum	Q1	Median	Q3	Max
10	1.6768	0.0309	0.1722	1.1992	1.5644	1.6971	1.7999	1.9369
20	1.7446	0.0274	0.1526	1.2605	1.7057	1.7664	1.8479	1.9496
30	1.7783	0.0259	0.1441	1.3436	1.7341	1.8055	1.8879	1.9604
40	1.8017	0.0253	0.1408	1.3984	1.7661	1.8355	1.9092	1.9723
50	1.8194	0.0242	0.1350	1.4385	1.7921	1.8589	1.9115	1.9709
60	1.8333	0.0233	0.1295	1.4514	1.8088	1.8785	1.9219	1.9711
70	1.8436	0.0224	0.1246	1.4686	1.8302	1.8824	1.9283	1.9688
80	1.8509	0.0216	0.1205	1.4868	1.8348	1.8883	1.9298	1.9664
90	1.8573	0.0211	0.1173	1.5063	1.8488	1.8995	1.9315	1.9675
100	1.8618	0.0207	0.1151	1.5267	1.8565	1.9007	1.9334	1.9702
110	1.8659	0.0203	0.1133	1.5473	1.8655	1.9080	1.9344	1.9697
120	1.8709	0.0203	0.1128	1.5659	1.8799	1.9131	1.9358	1.9705
130	1.8760	0.0202	0.1126	1.5682	1.8928	1.9216	1.9388	1.9695
140	1.8808	0.0201	0.1119	1.5743	1.8944	1.9298	1.9437	1.9715
150	1.8852	0.0201	0.1117	1.5769	1.8915	1.9311	1.9484	1.9755

Table 5: Higuchi fractal dimension statistics through K_{max} between 10 and 150 at intervals of 10 in the traffic noise protocol.

Property	Higuchi fractal dimension statistics (traffic noise exposure)							
K_{max}	Mean	SE mean	StDev	Minimum	Q1	Median	Q3	Max
10	1.6971	0.0279	0.1555	1.2606	1.6284	1.7171	1.8040	1.9496
20	1.7644	0.0265	0.1477	1.2952	1.7010	1.8077	1.8462	1.9383
30	1.7898	0.0256	0.1428	1.3544	1.7507	1.8447	1.8762	1.9450
40	1.8082	0.0242	0.1347	1.3912	1.7775	1.8533	1.8811	1.9579
50	1.8240	0.0227	0.1264	1.4132	1.8103	1.8590	1.9000	1.9703
60	1.8358	0.0217	0.1208	1.4290	1.8232	1.8741	1.9082	1.9691
70	1.8446	0.0214	0.1193	1.4368	1.8208	1.8879	1.9161	1.9722
80	1.8507	0.0212	0.1178	1.4372	1.8269	1.8934	1.9140	1.9762
90	1.8568	0.0210	0.1171	1.4337	1.8414	1.8922	1.9194	1.9804
100	1.8613	0.0209	0.1163	1.4326	1.8497	1.8990	1.9243	1.9837
110	1.8660	0.0207	0.1151	1.4383	1.8569	1.9076	1.9267	1.9824
120	1.8694	0.0203	0.1130	1.4474	1.8613	1.9121	1.9286	1.9811
130	1.8727	0.0200	0.1115	1.4597	1.8701	1.9103	1.9338	1.9831
140	1.8769	0.0197	0.1099	1.4732	1.8809	1.9070	1.9397	1.9810
150	1.8806	0.0193	0.1075	1.4888	1.8854	1.9066	1.9380	1.9795

Table 6: Higuchi fractal dimension at varying levels of K_{max} between 10 and 150 at equidistant intervals of 10.

Property	Higuchi fractal dimension statistics (control versus traffic)	
K_{max}	ANOVA1 (p value)	Kruskal-Wallis (p value)
10	0.6269	0.6322
20	0.6059	0.5543
30	0.7534	0.6523
40	0.8539	0.9215
50	0.8904	0.8880
60	0.9367	1.0000
70	0.9742	0.9215
80	0.9940	0.8108
90	0.9855	0.7675
100	0.9860	0.7568
110	0.9981	0.7354
120	0.9585	0.5082
130	0.9082	0.3041
140	0.8911	0.2910
150	0.8683	0.3175

The difference between these points is the interquartile range (IQR). Whiskers (or error bars) above and below the box indicate the 90th and 10th percentiles, respectively.

The levels of significance for parametric ANOVA1 and nonparametric Kruskal-Wallis test of significance for values of the Higuchi fractal dimension at varying levels of K_{max} between 10 and 150 at equidistant intervals of 10 are displayed in Table 6.

3.4. Five Entropies and DFA

3.4.1. ANOVA1 and Kruskal-Wallis Tests. Once more, we apply the Anderson-Darling and Lilliefors tests to the data to assess the normality. The results from both tests reveal similar numbers of nonnormal and normal distributions. So again we apply the Kruskal-Wallis and ANOVA1 tests of significance.

Table 7 reveals the mean values and standard deviation for the five entropic measures and DFA for the control and traffic noise exposure subjects RR intervals. The number of RR intervals is 500. ANOVA1 and Kruskal-Wallis test of significance were applied to results.

3.4.2. Principal Components Analysis. Here again we must complete a multivariate analysis. Shannon entropy has the First Principal Component (PC1) of 0.470, the Second Principal Component (PC2) of 0.258, and the Third Principal Component (PC3) of −0.245. But, Renyi entropy has the PC1 of 0.485, PC2 of 0.187, and PC3 of −0.200. However, Tsallis entropy has the PC1 of 0.472, PC2 of 0.249, and PC3 of −0.242.

Only the first three components need be considered due to the relatively steep scree plot. The cumulative influence as a percentage is 65.4 percent for the PC1 and 95.4 percent for the cumulative total of the PC1 and PC2. Finally, it is 99.3 percent for the cumulative total of the PC1, PC2, and PC3.

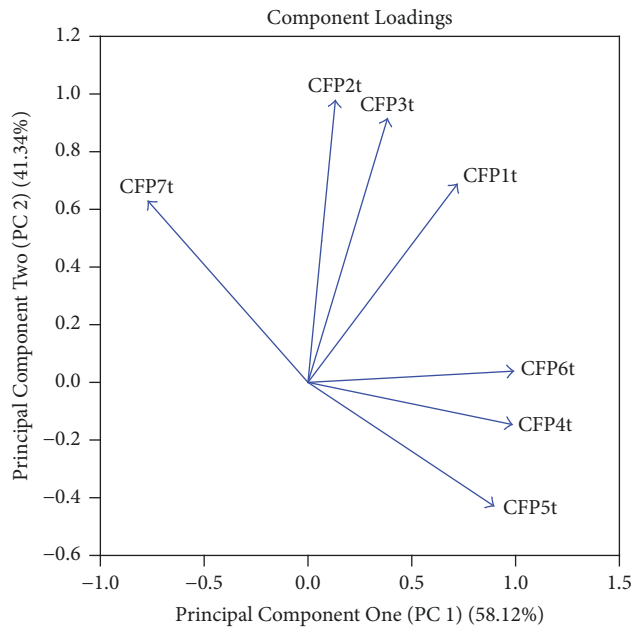

Figure 6: The plot illustrates the component loadings CFP1 to CFP7 for the 500 RR intervals of 31 traffic noise exposure subjects. The CFP values are deduced by using the MTM spectra throughout. The properties of the MTM spectra are as follows: sampling frequency 1 Hz, DPSS of 3, FFT length of 256, and Thomson's nonlinear combination at "adaptive." CFP1 and CFP3 are the most influential components when assessed by PCA.

PC2 has an influence of 30.0 percent. PC3 has an influence of 3.9 percent. So, Shannon, Renyi, and Tsallis are the optimal and most robust statistically overall combination regarding influencing the correct outcome. This is the case by means of the ANOVA1, Kruskal-Wallis, and the multivariate technique, hence PCA.

Table 8 illustrates the relevant Principal Component Analysis for five entropies and DFA of 31 traffic noise exposure subjects. The five entropy values and DFA are again deduced from 500 RR-interval time series.

4. Discussion

To provide further evidence regarding the interaction between auditory processing and the autonomic nervous system, we attempted to investigate whether acute exposure to traffic noise influenced the complexity of HRV. As a main outcome, we noticed that the traditional linear indices of HRV were unchanged during traffic noise exposure while some nonlinear approaches evidenced that the complexity of heart rate autonomic control increased during exposure to traffic noise.

In this context, previous studies suggest that noise exposure affects the sympathetic component of heart rate autonomic control [47, 48]. Tzaneva et al. [47] exposed subjects to 135 min of noise with Leq 95 dB (A) sound pressure and analyzed HRV before, during, and after noise exposure. They revealed an increase in the sympathetic regulation of heart rate under noise exposure. Björ et al. [48] investigated

Table 7: Entropic measures for the control and traffic nose exposure subjects RR intervals.

Entropy or DFA	Mean ± SD Control (n = 31)	Mean ± SD Traffic noise (n = 31)	ANOVA1 (p value)	Kruskal-Wallis (p value)	Effect size
Approximate	0.7443 ± 0.2354	0.7890 ± 0.2235	0.4465	0.3107	-
Sample	0.6923 ± 0.2300	0.7047 ± 0.2165	0.8278	0.8658	-
DFA	0.1722 ± 0.1943	0.1483 ± 0.1871	0.6222	0.6831	-
Shannon	0.5564 ± 0.1289	0.7017 ± 0.1272	<0.0001	<0.0001	1.13 (large)
Renyi	0.9840 ± 0.0058	0.9898 ± 0.0051	<0.0001	<0.0001	1.06 (large)
Tsallis	0.5981 ± 0.1193	0.7322 ± 0.1159	<0.0001	<0.0001	1.14 (large)

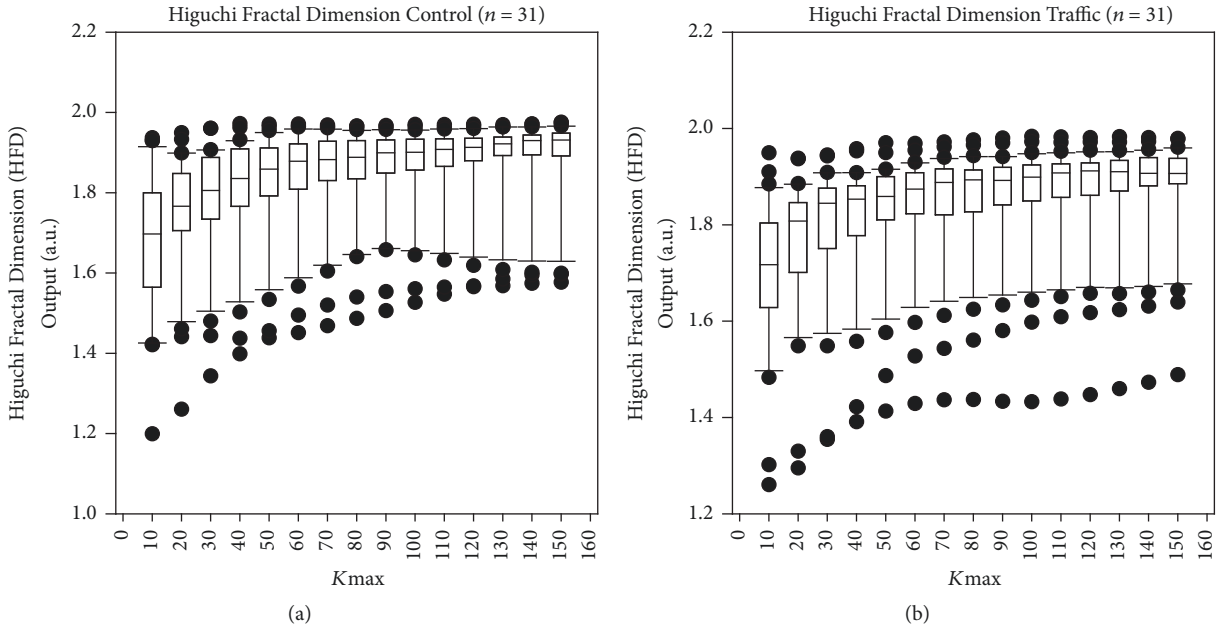

Figure 7: Box-and-whiskers plot for Higuchi fractal dimension of RR intervals of the control subjects (a) and the traffic noise exposure subjects (b), calculated multiple times from 10 to 150 in equidistant units for different levels of K_{max}.

healthy men and women and also noted increased values of the LF/HF ratio during noise exposure, indicating increased sympathetic control of heart rate.

Yet, an important point to be highlighted in their studies is the limitation of the LF/HF ratio to provide information regarding the sympathetic modulation of heart rate. The sympathovagal balance index that was added to their investigation, calculated by the LF/HF ratio, has been demonstrated to be theoretically flawed and empirically unsupported. Though many criticisms of this measure abound, the most serious concern is that LF index does not represent the sympathetic component. Thus, there is a lack of rationale and/or compelling evidence that its strength in relation to the HF index component would indicate relative strength of vagal and sympathetic signaling. Furthermore, the physiological significance of LF/HF ratio is erroneous and represents a superficial understanding of autonomic regulatory mechanisms [49–51]. We therefore emphasize that spectral analyses of HRV under controlled situations are the most effective markers of heart rate autonomic modulation. Yet, they do not accurately measure neural traffic or autonomic activity (i.e., pupil dilation, salivation, facial vasodilation, etc.).

Equally, Sim et al. [2] evaluated the effects of different noises on linear HRV. The authors enrolled 40 healthy men (23.9 ± 1.8 years old, and average BMI being 23.7 ± 2.1 kg/m^2) and submitted them to self-made traffic noise composed by aircraft and road traffic noise. The authors observed that traffic noise exposure increased SDNN and HF band in absolute units, indicating that traffic noise acutely increased HRV.

Although we did not observe any significant effects of traffic noise on time and frequency domain indices of HRV, we reported significant changes in the nonlinear parameters of HRV during traffic noise exposure. Entropic and chaotic global analysis of HRV revealed that the complexity of heart rate autonomic control increased during traffic noise exposure, suggesting increasing randomness in the system.

According to our findings, Shannon entropy values increased (large effect size) during traffic noise exposure.

Table 8: The relevant Principal Component Analysis for five entropies and DFA of 31 traffic noise exposure subjects.

Entropy (or DFA)	PC1	PC2	PC3
Approximate	0.397	−0.415	0.497
Sample	0.405	−0.419	0.307
DFA	0.007	0.700	0.708
Shannon	0.470	0.258	−0.245
Renyi	0.485	0.187	−0.200
Tsallis	0.472	0.249	−0.242

Entropy is theoretically related to the amount of disorder of particles in a system; if the entropy decreases, the predictability of the process increases and the system becomes less complex [52]. The Shannon entropy quantifies the complexity of a system by means of an average information content [52]. In a recent study, heart beat time series were quantified by Shannon entropy and decreased values were associated with increased severity of pathological condition [53]. Also, decreased Shannon entropy values were found in leprosy victims when HRV was investigated [54].

We also revealed that Renyi entropy values were higher during exposure to traffic noise (large effect size). The Renyi entropy generalizes the Shannon entropy and considers the Shannon entropy as a singular case [55]. The Renyi entropy was previously reported to identify cardiac autonomic neuropathy [56]. It was recently shown as an effective method in real-time monitoring of atrial fibrillation patients and for prediction and diagnosis of paroxysmal atrial fibrillation [57].

Based on our data, Tsallis entropy analysis confirmed that the complexity of HRV increased during traffic noise exposure and Cohen's d calculation exhibited large effect size. This nonlinear approach is not chiefly used in HRV analysis; Eduardo Virgilio Silva and Otavio Murta [58] applied Tsallis entropy in time series and suggested it as a potential method for complexity system analysis, thus supporting our conclusions.

Our results demonstrated through chaotic global analysis of HRV that CFP3 and CFP6 significantly increased (large effect size) during traffic noise exposure, indicating higher complexity of RR-intervals oscillations during auditory stimulation. A previous study reported that chaotic global analysis was unable to identify HRV changes during mental task [59]. Another research study investigated chaotic global analysis in RR intervals during exposure to heavy metal music [60]. The authors failed to reveal influences of this music style on the complexity of HRV.

Nonlinear analysis of HRV is a complex issue owing to its physiological interpretation. Conversely, the literature shows that decreased complexity of HRV represents a physiological impairment. Accordingly, our data points to an interesting interpretation that acute traffic noise exposure in a laboratory situation does not cause stressful autonomic responses. An elegant systematic review reported that the majority of studies performed at the roadside evidenced stressful effects of traffic noise on cardiovascular, respiratory, and metabolic health [61]. However, in view of our results, we deduced that the stress induced by exposure to road traffic noise is not only due to the auditory stimulus but due to the roadside environmental situation.

The interaction between auditory processing and heart rate autonomic control has been reviewed before [62]. Nakamura et al. [63] reported that auditory stimulation influenced renal sympathetic nerve activity and blood pressure in anesthetized rats. The same researchers observed that vagal gastric nerve activity was similarly influenced by music [64]. The authors indicated that the suprachiasmatic nucleus of the hypothalamus is involved in this process [63].

Amongst the important points to be addressed in our study, we allow for the laboratory conditions the volunteers were exposed to. This is because we intended to discard the influence of the traffic environmental impact on HRV, that is, pollution, visual stimulation, and conversation. We investigated only women in order to avoid influence of sexual hormones. We believe that a combination of different factors during traffic noise stimulus would induce tougher effects on HRV, since the ANS is sensitive to innumerous exogenous elements [14].

The luteal and follicular phase of the menstrual cycle were also controlled, since there is previous evidence of its influence on nonlinear HRV [11].

Another fact worth highlighting is that, in our study, nonlinear methods of HRV were more sensitive at detecting changes in the RR-interval fluctuations. This is possibly because some information may be erroneous if only linear analysis is undertaken. Nonlinear analysis was revealed to be a more powerful approach to identify complex systems [9].

5. Conclusion

Traffic noise exposure did not significantly alter linear indices of HRV. Higuchi fractal dimension, DFA, and Approximate and Sample entropies were similarly significantly unaffected. Yet, it significantly changed chaotic global analysis (combinations CFP3 and CFP6) and Shannon, Renyi, and Tsallis entropies. Our results indicate that traffic noise acutely enhances the complexity of heart rate autonomic control in healthy women.

Conflicts of Interest

The authors declare that there are no conflicts of interest regarding the publication of this paper.

Acknowledgments

This study received financial support from FAPESP (Process no. 2012/01366-6 and 2018/02664-7).

References

[1] T. B. Lonsdorf and C. J. Merz, "More than just noise: Inter-individual differences in fear acquisition, extinction and return of fear in humans-biological, experiential, temperamental factors, and methodological pitfalls," *Neuroscience & Biobehavioral Reviews*, vol. 80, pp. 703–728, 2017.

[2] C. S. Sim, J. H. Sung, S. H. Cheon, J. M. Lee, J. W. Lee, and J. Lee, "The effects of different noise types on heart rate variability in men," *Yonsei Medical Journal*, vol. 56, no. 1, pp. 235–243, 2015.

[3] G.-S. Lee, M.-L. Chen, and G.-Y. Wang, "Evoked response of heart rate variability using short-duration white noise," *Autonomic Neuroscience: Basic and Clinical*, vol. 155, no. 1-2, pp. 94–97, 2010.

[4] M. Umemura and K. Honda, "Influence of music on heart rate variability and comfort," *Journal of Human Ergology*, vol. 27, pp. 30–38, 1998.

[5] O. K. A. Lee, Y. F. L. Chung, M. F. Chan, and W. M. Chan, "Music and its effect on the physiological responses and anxiety levels of patients receiving mechanical ventilation: A pilot study," *Journal of Clinical Nursing*, vol. 14, no. 5, pp. 609–620, 2005.

[6] M. Fernandes de Godoy, "Nonlinear Analysis of Heart Rate Variability: A Comprehensive Review," *Journal of Cardiology and Therapy*, vol. 3, no. 3, pp. 528–533, 2016.

[7] A. Voss, S. Schulz, R. Schroeder, M. Baumert, and P. Caminal, "Methods derived from nonlinear dynamics for analysing heart rate variability," *Philosophical Transactions of the Royal Society A: Mathematical, Physical & Engineering Sciences*, vol. 367, no. 1887, pp. 277–296, 2009.

[8] B. Francesco, B. Maria Grazia, and G. Emanuele, "Linear and nonlinear heart rate variability indexes in clinical practice," *Computational and Mathematical Methods in Medicine*, vol. 2012, Article ID 219080, 5 pages, 2012.

[9] R. Sassi, S. Cerutti, F. Lombardi et al., "Advances in heart rate variability signal analysis: joint position statement by the e-Cardiology ESC Working Group and the European Heart Rhythm Association co-endorsed by the Asia Pacific Heart Rhythm Society," *EP Europace*, vol. 17, no. 9, pp. 1341–1353, 2015.

[10] H. V. Huikuri, T. H. Mäkikallio, and J. Perkiömäki, "Measurement of heart rate variability by methods based on nonlinear dynamics," *Journal of Electrocardiology*, vol. 36, pp. 95–99, 2003.

[11] X. Bai, J. Li, L. Zhou, and X. Li, "Influence of the menstrual cycle on nonlinear properties of heart rate variability in young women," *American Journal of Physiology-Heart and Circulatory Physiology*, vol. 297, no. 2, pp. H765–H774, 2009.

[12] A. L. Roque, V. E. Valenti, H. L. Guida et al., "The effects of different styles of musical auditory stimulation on cardiac autonomic regulation in healthy women," *Noise & Health*, vol. 15, no. 65, pp. 281–287, 2013.

[13] A. L. Roque, V. E. Valenti, H. L. Guida et al., "The effects of auditory stimulation with music on heart rate variability in healthy women," *Clinics*, vol. 68, no. 7, pp. 960–967, 2013.

[14] A. J. Camm, M. Malik, J. T. Bigger et al., "Heart rate variability: standards of measurement, physiological interpretation and clinical use," *Task Force of the European Society of Cardiology and the North American Society of Pacing and Electrophysiology. Circulation*, vol. 93, pp. 1043–1065, 1996.

[15] C.-K. Peng, S. Havlin, H. E. Stanley, and A. L. Goldberger, "Quantification of scaling exponents and crossover phenomena in nonstationary heartbeat time series," *Chaos: An Interdisciplinary Journal of Nonlinear Science*, vol. 5, no. 1, pp. 82–87, 1995.

[16] G. C. Donaldson, T. A. R. Seemungal, J. R. Hurst, and J. A. Wedzicha, "Detrended fluctuation analysis of peak expiratory flow and exacerbation frequency in COPD," *European Respiratory Journal*, vol. 40, no. 5, pp. 1123–1129, 2012.

[17] P. Castiglioni, L. Quintin, A. Civijian, G. Parati, and M. Di Rienzo, "Local-scale analysis of cardiovascular signals by detrended fluctuations analysis: Effects of posture and exercise," in *Proceedings of the Engineering in Medicine and Biology Society, EMBS 29th Annual International Conference of the IEEE*, pp. 5035–5038, 2007.

[18] R. Karasik, N. Sapir, Y. Ashkenazy et al., "Correlation differences in heartbeat fluctuations during rest and exercise," *Physical Review E: Statistical, Nonlinear, and Soft Matter Physics*, vol. 66, no. 6, Article ID 062902, p. 062902/4, 2002.

[19] R. De Leon-Lomeli, J. S. Murguia, I. Chouvarda et al., "Relation between heart beat fluctuations and cyclic alternating pattern during sleep in insomnia patients," in *Proceedings of the Engineering in Medicine and Biology Society (EMBC), 36th Annual International Conference of the IEEE*, pp. 2249–2252, 2014.

[20] C.-M. Liao, N.-H. Hsieh, and C.-P. Chio, "Fluctuation analysis-based risk assessment for respiratory virus activity and air pollution associated asthma incidence," *Science of the Total Environment*, vol. 409, no. 18, pp. 3325–3333, 2011.

[21] R. C. Rossi, F. M. Vanderlei, A. F. Bernardo et al., "Effect of pursed-lip breathing in patients with COPD: Linear and nonlinear analysis of cardiac autonomic modulation," *Copd-Journal of Chronic Obstructive Pulmonary Disease*, vol. 11, no. 1, pp. 39–45, 2014.

[22] J. Annegarn, M. Spruit, H. Savelberg et al., "Stride time fluctuations during the six minute walk test in COPD patients," in *Proceedings of the Rehabilitation: Mobility, Exercise, and Sports: 4th International State-of-the-Art Congress*, p. 149, IOS Press, 2010.

[23] M. Ghil, "The SSA-MTM toolkit: Applications to analysis and prediction of time series," *Applications of Soft Computing*, pp. 216–230, 1997.

[24] D. Slepian, "Prolate Spheroidal Wave Functions, Fourier Analysis, and Uncertainty—V: The Discrete Case," *Bell System Technical Journal*, vol. 57, no. 5, pp. 1371–1430, 1978.

[25] S. H. Gould, *Variational methods for eigenvalue problems: an introduction to the methods of Rayleigh, Ritz, Weinstein, and Aronszajn*, Courier Dover Publications, 1995.

[26] R. Wajnsztejn, T. D. De Carvalho, D. M. Garner et al., "Heart rate variability analysis by chaotic global techniques in children with attention deficit hyperactivity disorder," *Complexity*, vol. 21, no. 6, pp. 412–419, 2016.

[27] D. M. Garner and B. W.-K. Ling, "Measuring and locating zones of chaos and irregularity," *Journal of Systems Science and Complexity*, vol. 27, no. 3, pp. 494–506, 2014.

[28] C. E. Shannon, "A mathematical theory of communication," *Bell Labs Technical Journal*, vol. 27, pp. 379–423, 623–656, 1948.

[29] R. J. dos Santos, "Generalization of Shannon's theorem for Tsallis entropy," *Journal of Mathematical Physics*, vol. 38, no. 8, pp. 4104–4107, 1997.

[30] E. K. Lenzi, R. S. Mendes, and L. R. Da Silva, "Statistical mechanics based on Renyi entropy," *Physica A: Statistical Mechanics and its Applications*, vol. 280, no. 3, pp. 337–345, 2000.

[31] A. E. Taylor, "L'Hospital's rule," *The American Mathematical Monthly*, vol. 59, pp. 20–24, 1952.

[32] I. Pinelis, "L'Hospita Type rules for monotonicity, with applications," *Journal of Inequalities in Pure andApplied Mathematics*, no. 3, 2002.

[33] K. Zyczkowski, "Rényi extrapolation of Shannon entropy," *Open Systems and Information Dynamics*, vol. 10, no. 3, pp. 297–310, 2003.

[34] A. R. Plastino and A. Plastino, "Stellar polytropes and Tsallis' entropy," *Physics Letters A*, vol. 174, no. 5-6, pp. 384–386, 1993.

[35] A. M. Mariz, "On the irreversible nature of the Tsallis and Renyi entropies," *Physics Letters A*, vol. 165, no. 5-6, pp. 409–411, 1992.

[36] S. M. Pincus, "Approximate entropy as a measure of system complexity," *Proceedings of the National Acadamy of Sciences*, vol. 88, no. 6, pp. 2297–2301, 1991.

[37] J. S. Richman and J. R. Moorman, "Physiological time-series analysis using approximate entropy and sample entropy," *American Journal of Physiology-Heart and Circulatory Physiology*, vol. 278, no. 6, pp. H2039–H2049, 2000.

[38] M. P. Tarvainen, J.-P. Niskanen, J. A. Lipponen, P. O. Ranta-aho, and P. A. Karjalainen, "Kubios HRV—heart rate variability analysis software," *Computer Methods and Programs in Biomedicine*, vol. 113, no. 1, pp. 210–220, 2014.

[39] J. S. Richman, D. E. Lake, and J. R. Moorman, "Sample Entropy," *Methods in Enzymology*, vol. 384, pp. 172–184, 2004.

[40] T. Higuchi, "Approach to an irregular time series on the basis of the fractal theory," *Physica D: Nonlinear Phenomena*, vol. 31, no. 2, pp. 277–283, 1988.

[41] M. J. Katz, "Fractals and the analysis of waveforms," *Computers in Biology and Medicine*, vol. 18, no. 3, pp. 145–156, 1988.

[42] P. Castiglioni, "What is wrong in Katz's method? Comments on: "A note on fractal dimensions of biomedical waveforms"," *Computers in Biology and Medicine*, vol. 40, no. 11-12, pp. 950–952, 2010.

[43] J. E. Skinner, C. M. Pratt, and T. Vybiral, "A reduction in the correlation dimension of heartbeat intervals precedes imminent ventricular fibrillation in human subjects," *American Heart Journal*, vol. 125, no. 3, pp. 731–743, 1993.

[44] P. Van Leeuwen, H. Bettermann, U. An der Heiden, and H. C. Kummell, "Circadian aspects of apparent correlation dimension in human heart rate dynamics," *American Journal of Physiology-Heart and Circulatory Physiology*, vol. 269, no. 1, pp. H130–H134, 1995.

[45] T. Q. D. Khoa, V. Q. Ha, and V. V. Toi, "Higuchi fractal properties of onset epilepsy electroencephalogram," *Computational and Mathematical Methods in Medicine*, vol. 2012, 2012.

[46] D. S. Quintana, "Statistical considerations for reporting and planning heart rate variability case-control studies," *Psychophysiology*, vol. 54, no. 3, pp. 344–349, 2017.

[47] L. Tzaneva, S. Danev, and R. Nikolova, "Investigation of noise exposure effect on heart rate variability parameters," *Central European Journal of Public Health*, vol. 9, no. 3, pp. 130–132, 2001.

[48] B. Björ, L. Burström, M. Karlsson, T. Nilsson, U. Näslund, and U. Wiklund, "Acute effects on heart rate variability when exposed to hand transmitted vibration and noise," *International Archives of Occupational and Environmental Health*, vol. 81, no. 2, pp. 193–199, 2007.

[49] G. E. Billman, "The LF/HF ratio does not accurately measure cardiac sympatho-vagal balance," *Frontiers in Physiology*, vol. 4, article 26, 2013.

[50] J. A. J. Heathers, "Sympathovagal balance from heart rate variability: An obituary," *Experimental Physiology*, vol. 97, no. 4, pp. 556-556, 2012.

[51] D. S. Goldstein, O. Bentho, M.-Y. Park, and Y. Sharabi, "Low-frequency power of heart rate variability is not a measure of cardiac sympathetic tone but may be a measure of modulation of cardiac autonomic outflows by baroreflexes," *Experimental Physiology*, vol. 96, no. 12, pp. 1255–1261, 2011.

[52] T. M. Cover and J. A. Thomas, *Elements of information theory*, 2nd edition, 2006.

[53] M. Vallverdu, F. Claria, U. Melia, A. B. De Luna, and P. Caminal, "Measuring heart rate variability by means of information entropies based on Choi-Williams distribution," in *Proceedings of the Engineering in Medicine and Biology Society (EMBC), 37th Annual International Conference of the IEEE*, pp. 1797–1800, 2015.

[54] M. C. D. S. Santos, L. C. D. L. Silveira, S. C. G. Moura-Tonello, A. Porta, A. M. Catai, and G. D. S. Souza, "Heart rate variability in multibacillar leprosy: Linear and nonlinear analysis," *PLoS ONE*, vol. 12, no. 7, Article ID e0180677, 2017.

[55] R. Alfréd, "On measures of information and entropy," in *Proceedings of the 4th Berkeley Symposium on Mathematics, Statistics and Probability*, pp. 547–561, 1960.

[56] D. J. Cornforth, M. P. Tarvainen, and H. F. Jelinek, "How to Calculate Renyi Entropy from Heart Rate Variability, and Why it Matters for Detecting Cardiac Autonomic Neuropathy," *Frontiers in Bioengineering and Biotechnology*, vol. 2, 2014.

[57] Y. Xin, Y. Zhao, Y. Mu, Q. Li, and C. Shi, "Paroxysmal atrial fibrillation recognition based on multi-scale Rényi entropy of ECG," *Technology and Health Care*, vol. 25, no. 1, pp. S189–S196, 2017.

[58] L. Eduardo Virgilio Silva and L. Otavio Murta, "Evaluation of physiologic complexity in time series using generalized sample entropy and surrogate data analysis," *Chaos: An Interdisciplinary Journal of Nonlinear Science*, vol. 22, no. 4, Article ID 043105, 2012.

[59] A. M. G. Fontes, D. M. Garner, L. C. de Abreu et al., "Global chaotic parameters of heart rate variability during mental task," *Complexity*, vol. 21, no. 5, pp. 300–307, 2016.

[60] M. L. Nogueira, D. M. Garner, E. Osório, L. C. Abreu, and V. E. Valenti, "Globally chaotic analysis of Heart Rate Variability during acute auditory stimulus by heavy metal music," *Medical Express*, vol. 2, no. 5, 2015.

[61] A. Recio, C. Linares, J. R. Banegas, and J. Díaz, "Road traffic noise effects on cardiovascular, respiratory, and metabolic health: An integrative model of biological mechanisms," *Environmental Research*, vol. 146, pp. 359–370, 2016.

[62] V. E. Valenti, H. L. Guida, A. C. F. Frizzo, A. C. V. Cardoso, L. C. M. Vanderlei, and L. C. de Abreu, "Auditory stimulation and cardiac autonomic regulation," *Clinics*, vol. 67, no. 8, pp. 955–958, 2012.

[63] T. Nakamura, M. Tanida, A. Niijima, H. Hibino, J. Shen, and K. Nagai, "Auditory stimulation affects renal sympathetic nerve activity and blood pressure in rats," *Neuroscience Letters*, vol. 416, no. 2, pp. 107–112, 2007.

[64] T. Nakamura, M. Tanida, A. Niijima, and K. Nagai, "Effect of auditory stimulation on parasympathetic nerve activity in urethane-anesthetized rats," *In Vivo*, vol. 23, no. 3, pp. 415–420, 2009.